Supporting Information

Negative differential resistance effect in resistive switching devices based on *h*-$LuFeO_3$/$CoFe_2O_4$ heterojunctions

Xinxin Ran,[1] Pengfei Hou,[1,2,*] Jiaxun Song,[1] Hongjia Song,[1] Xiangli Zhong[1] and Jinbin Wang[1,*]

[1] *School of Materials Science and Engineering, Xiangtan University, Hunan Xiangtan 411105, China*

[2] *Science and Technology on Reliability Physics and Application Technology of Electronic Component Laboratory, Guangdong Guangzhou 510610, China*

Table S1. Growth parameters of the *h*-LFO/CFO/SRO/CFO heterostructures.

Layer	*h*-LFO	CFO	SRO	CFO
Method	PLD	PLD	PLD	PLD
Deposition time	60 min	3 min	30 min	10 min
Atmosphere	Oxygen	Oxygen	Oxygen	Oxygen
Oxygen pressure	100 mTorr	50 mTorr	80 mTorr	50 mTorr
Temperature	720°C	600°C	690°C	600°C
Frequency	10 Hz	10 Hz	10 Hz	10 Hz
Power	1.39 W	1.96 W	1.49 W	1.96 W
Laser energy	400 mJ	350 mJ	350 mJ	350 mJ

Selection of experimental parameters

During the deposition process, when the incident energy of the laser is fixed, the kinetic energy of

* *Corresponding author: Electronic mail houpf@xtu.edu.cn and jbwang@xtu.edu.cn.*

the atom is mainly determined by the temperature. The energy is insufficient to move the atoms to the lowest energy position to nucleate at lower growth temperatures.[1] However, the anti-evaporation phenomenon may appear if the temperature is pretty high, which can reduce the crystal quality of the thin film. On the other hand, we hope to achieve low temperature growth, which is beneficial to the practical application and the reduction of energy consumption. It has been reported that the growth temperature is range from 500 ℃ to 700 °C for CFO.[2] The low growth temperature means that the surface is easy to accumulate into islands when the migration rate is less than the deposition rate, which may generate plenty of defects. However, it may also lead to the formation of conductive filaments when a large number of defects exist, and the interface may no longer play a major role in our samples. Moreover, it is hard to crystallize for CFO when the temperature is pretty low. Thus, the growth temperature was chosen as 600 ℃. The proper growth temperature range of *h*-LFO is 650 ℃ ~ 800 ℃ according to our previous report, and the higher temperatures may lead to the formation of heterogeneous phases.[1] However, much low growth temperature may also cause poor crystal quality and ferroelectricity. Therefore, we chose a growth temperature of 720 ℃, which can satisfy the crystal quality as well as low temperature. According to our results, the further increase of temperature below 800 ℃ may help to improve the ferroelectricity of *h*-LFO, and the higher ON/OFF ratio may be obtained. In addition, increasing the growth temperature of CFO properly may generate more defects at the interface of *h*-LFO/CFO/SRO, which may lead to more obvious NDR effect.

The oxygen pressure during the deposition of oxide film will greatly affect the film crystal structure, conductivity, and charge transport properties in oxides.[3, 4] The relatively high oxygen pressure tends to form a rough surface, which is beneficial to the formation of interfacial defects.[5]

While it is not conducive to the growth of *h*-LFO when the surface of the CFO buffer layer is too rough. The CFO grown at 600℃ and 40 mTorr has some kind of very small porosities and voids.[5] Therefore, in order to obtain the interfacial defects while do not affect the growth of CFO, the oxygen pressure was set as 50 mTorr. Higher oxygen pressure is beneficial to reduce the oxygen vacancy concentration in *h*-LFO film and improve the ferroelectric properties.[6] But when the oxygen pressure is too high, the probability of plume colliding with oxygen is large, which causes the larger energy loss, so that the plume does not have enough energy to reach a suitable substrate position, and makes it hard to form the hexagonal phases. Thus, the oxygen pressure was set as 100 mTorr to ensure the ferroelectricity of *h*-LFO, which is higher than that had ever been reported.[7] Increasing the oxygen pressure properly will help to eliminate internal oxygen vacancies and improve ferroelectric properties.

The thickness of ferroelectric layer has a great influence on the strength of interface effect. When the thickness of the ferroelectric layer is too thin, and the modulation effect of ferroelectric polarization on the depletion layer decreases.[8] In contrast, although the modulation effect of ferroelectric polarization on the depletion layer may become powerful in thicker films, the conductive property of ferroelectric films tends to decrease with increasing thickness.[9] In this situation, the volume resistance becomes more crucial than the interfacial effect. Thus, the thickness of *h*-LFO was controlled to tens of nanometers. It can not only ensure to obtain better ferroelectric properties, but also make the conduction be dominated by the interface. The thicker CFO may be beneficial to obtain the higher ON/OFF ratio. However, it may also lead to the worse ferroelectricity of our samples because of the larger depolarization field.[10] Furthermore, the thicker CFO means the more internal defects may exist, which can lead to the stronger trapping effect. Therefore, the growth

time of CFO was controlled to 3 minutes and the thickness was controlled to several nanometers. On one hand, the heterojunction can achieve better ferroelectric properties, on the other hand, the RS and NDR effects can be realized.

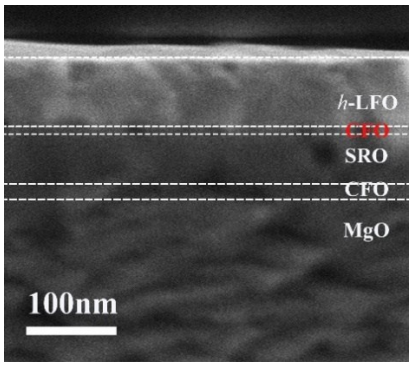

Figure S1. The cross-sectional SEM image of *h*-LFO/CFO/SRO/CFO/MgO heterostructure.

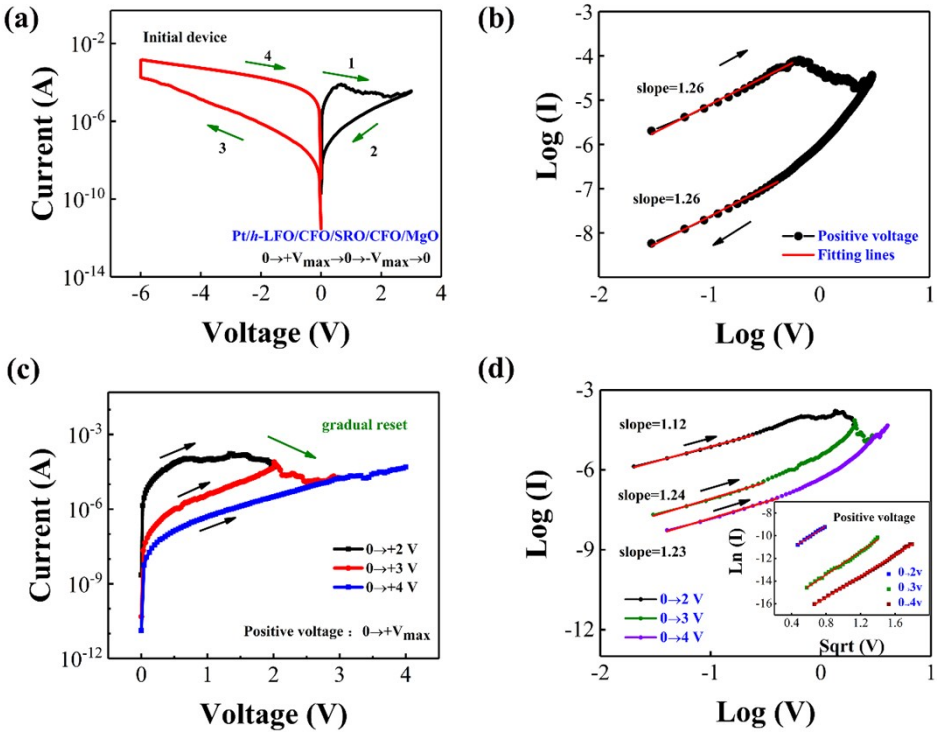

Figure S2. Resistive switching characteristics in the original device. (a) The *I*-*V* curve of the original Pt/*h*-LFO/CFO/SRO/CFO/MgO device. (b) log(*I*)-log(*V*) curve under forward voltage. (c) *I*-*V* and (d) log(*I*)-log(*V*) curves at 0→2 V, 0→3 V, 0→4 V, respectively (illustrated as Schottky emission

fitting).

The F-N tunneling model can be described by the following equation:[11]

$$J = \frac{q^3 E^2}{8\pi h \varphi_B} exp(\frac{-8\pi(2m^*)^{1/2}}{3qhE}) \quad (1)$$

where J is the current density, q is the electron charge, E is the electric field, φ_B is the height of Schottky potential barrier, h is Planck's constant, m^* is the effective mass of electron. According to equation 1, the plots of $\ln(I/V^2)$ versus $1/V$ for high resistance states in positive and negative high-voltage region are shown in **Figure S3**.

The Schottky emission model can be described by the following equation:[12]

$$J = A^* T^2 exp(\frac{-q\varphi_B}{kT} + \frac{\sqrt{qE/4\pi\varepsilon\varepsilon_0}}{kT}) \quad (2)$$

where A^* the Richardson constant, T is the temperature, k is the Boltzmann's constant, q is the electron charge, E is the electric field, ε is the dielectric constant, ε_0 is the vacuum dielectric constant. If the mechanism is consistent with F-N tunneling, the $\ln(I/V^2)$-$1/V$ curve should be a straight line, however, the fitting results show the nonlinear behavior and the F-N tunneling can be excluded. Therefore, the conduction may be mainly dominated by the Schottky emission. The plots of $\ln(I)$ versus $V^{1/2}$ are shown in **Figure S4,** which illustrate the domination of Schottky emission model.

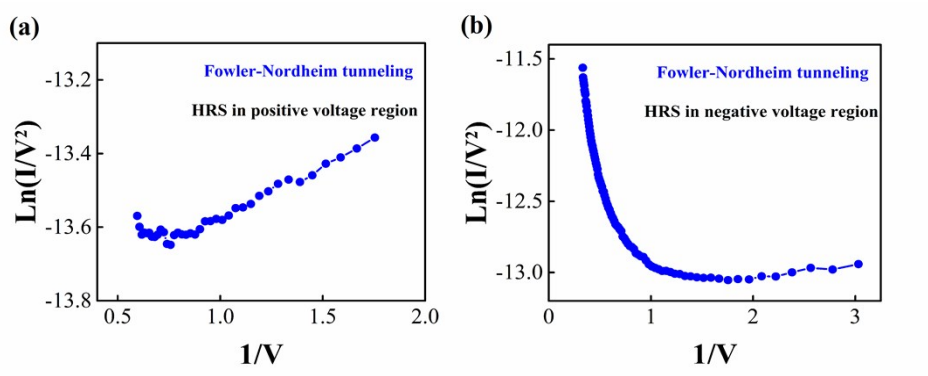

Figure S3. Fitting results of F-N tunneling for HRS in (a) positive voltage and (b) negative voltage region.

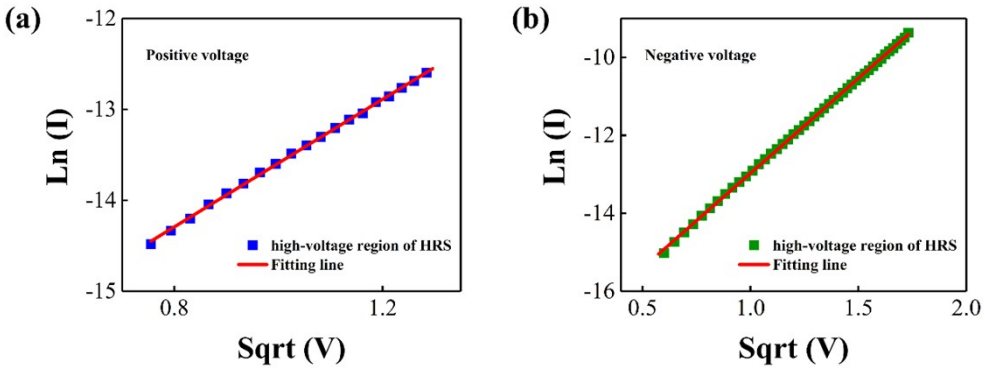

Figure S4. Fitting results of Schottky emission in (a) positive voltage and (b) negative voltage region.

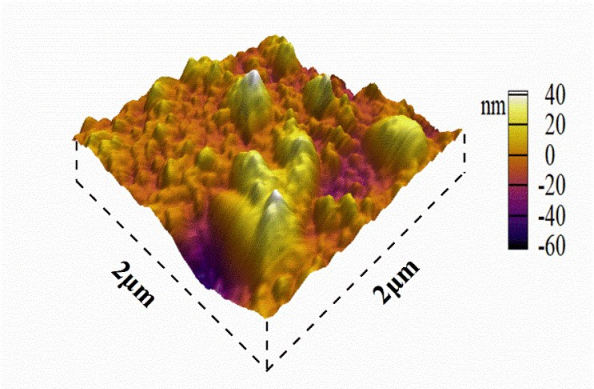

Figure S5. The AFM pattern of Pt electrode after annealing at 300 °C.

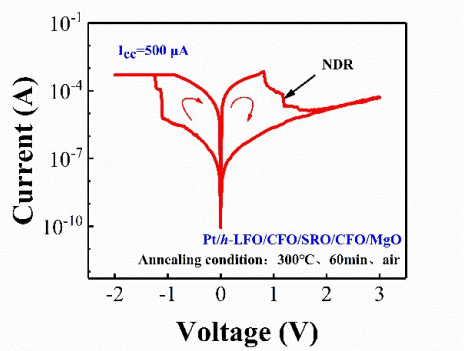

Figure S6. The *I-V* characteristic of Pt/*h*-LFO/CFO/SRO/CFO/MgO device after annealing at 300 °C.

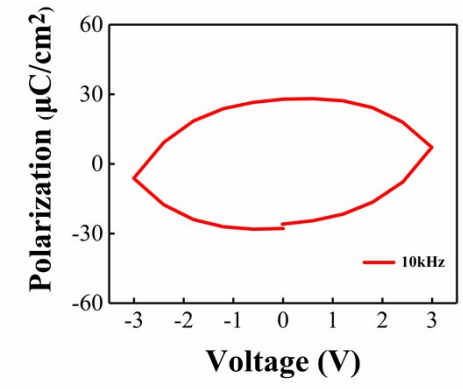

Figure S7. The *P-V* curve of Pt/*h*-LFO/CFO/SRO/CFO/MgO devices after annealing at 300 °C.

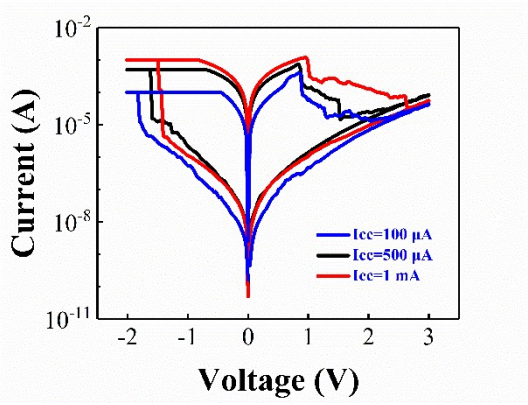

Figure S8. The *I-V* curves at different compliance currents of Pt/*h*-LFO/CFO/SRO/CFO/MgO devices after annealing at 300 °C.

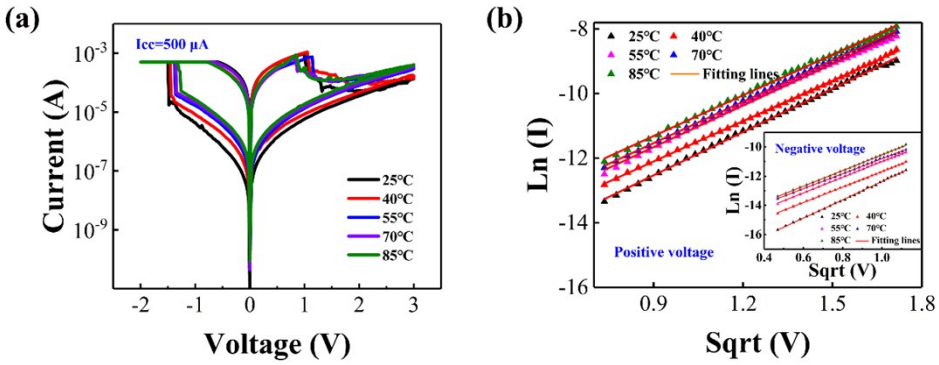

Figure S9. The *I-V* curves at different temperatures, (b) Schottky fitting results of HRS in the positive and negative voltage region.

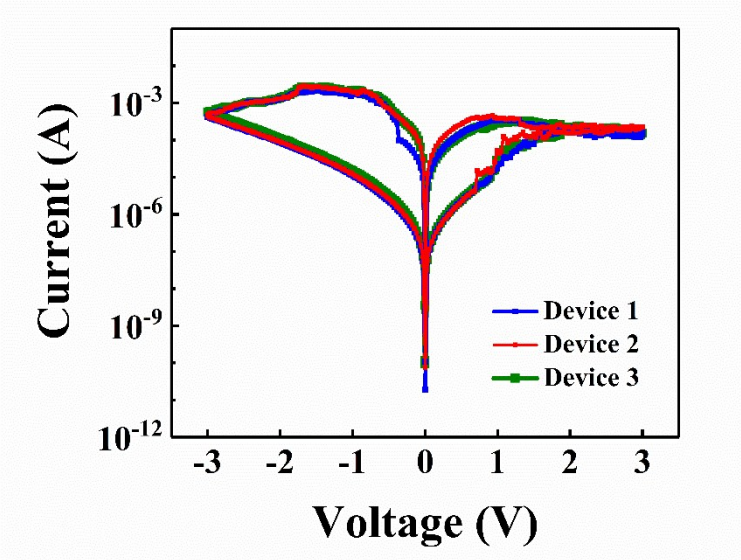

Figure S10. The *I-V* curves of 3 samples as a consequence of 0 V→+3 V→0 V→-3 V→0 V.

References

1. X. Zhang, H. Song, C. Tan, S. Yang, Y. Xue, J. Wang and X. Zhong, *Journal of Materials Science*, 2017, **52**, 13879-13885.
2. J.-p. Zhou, H.-c. He and C.-W. Nan, *Applied surface science*, 2007, **253**, 7456-7460.
3. T. Zhao, F. Chen, H. Lu, G. Yang and Z. Chen, *Journal of Applied Physics*, 2000, **87**, 7442-7447.
4. T. Zhao, Z.-H. Chen, F. Chen, H.-B. Lu, G.-Z. Yang and H.-S. Cheng, *Applied Physics Letters*, 2000, **77**, 4338-4340.
5. M. Khodaei, S. S. Ebrahimi, Y. J. Park, J. M. Ok, J. S. Kim, J. Son and S. Baik, *Journal of magnetism and magnetic materials*, 2013, **340**, 16-22.
6. M. Li, J. Zhou, X. Jing, M. Zeng, S. Wu, J. Gao, Z. Zhang, X. Gao, X. Lu and J. M. Liu, *Advanced Electronic Materials*, 2015, **1**, 1500069.
7. J. A. Moyer, R. Misra, J. A. Mundy, C. M. Brooks, J. T. Heron, D. A. Muller, D. G. Schlom and P. Schiffer, *Apl Materials*, 2014, **2**, 012106.
8. Y. Bai, Z. J. Wang, Y. N. Chen and J. Z. Cui, *ACS applied materials & interfaces*, 2016, **8**, 32948-32955.
9. Z. J. Wang and Y. Bai, *Small*, 2019, **15**, 1805088.
10. A. Tsurumaki-Fukuchi, H. Yamada and A. Sawa, *Applied Physics Letters*, 2013, **103**, 152903.
11. R. H. Fowler and L. Nordheim, *Proceedings of the Royal Society of London. Series A, Containing Papers of a Mathematical and Physical Character*, 1928, **119**, 173-181.
12. C. Chaneliere, J. Autran, R. Devine and B. Balland, *Materials Science and Engineering: R: Reports*, 1998, **22**, 269-322.